

Effect of pseudouridylation on the structure and activity of the catalytically essential P6.1 hairpin in human telomerase RNA

Nak-Kyoon Kim¹, Carla A. Theimer¹, James R. Mitchell², Kathleen Collins² and Juli Feigon^{1,*}

¹Department of Chemistry and Biochemistry, University of California, Los Angeles, CA 90095 and

²Department of Molecular and Cell Biology, University of California, Berkeley, CA 94720, USA

Received April 9, 2010; Revised May 21, 2010; Accepted May 24, 2010

ABSTRACT

Telomerase extends the 3'-ends of linear chromosomes by adding conserved telomeric DNA repeats and is essential for cell proliferation and genomic stability. Telomerases from all organisms contain a telomerase reverse transcriptase and a telomerase RNA (TER), which together provide the minimal functional elements for catalytic activity *in vitro*. The RNA component of many functional ribonucleoproteins contains modified nucleotides, including conserved pseudouridines (Ψ s) that can have subtle effects on structure and activity. We have identified potential Ψ modification sites in human TER. Two of the predicted Ψ s are located in the loop of the essential P6.1 hairpin from the CR4-CR5 domain that is critical for telomerase catalytic activity. We investigated the effect of P6.1 pseudouridylation on its solution NMR structure, thermodynamic stability of folding and telomerase activation *in vitro*. The pseudouridylated P6.1 has a significantly different loop structure and increase in stability compared to the unmodified P6.1. The extent of loop nucleotide interaction with adjacent residues more closely parallels the extent of loop nucleotide evolutionary sequence conservation in the Ψ -modified P6.1 structure. Pseudouridine-modification of P6.1 slightly attenuates telomerase activity but slightly increases processivity *in vitro*. Our results suggest that Ψ s could have a subtle influence on human telomerase activity via impact on TER-TERT or TER-TER interactions.

INTRODUCTION

Pseudouridine (Ψ , Figure 1A) is the most abundant post-transcriptionally modified nucleotide found in cellular RNAs of all species, and the locations of the Ψ s are often highly conserved across phylogeny (1,2). Pseudouridine is an isomer of uridine with a C5-C1' glycosidic bond, which provides an additional imino group (Ψ N1H) for hydrogen bonding. Pseudouridines are found in functionally important regions of rRNA, tRNA and small nuclear RNA (snRNA), and have been shown to play subtle but important roles in biological function (3). For example, Ψ s stabilize the tertiary structure of tRNAs through base-stacking interactions (4–7). A conserved Ψ in the eukaryotic U2 snRNA has been shown to affect the conformation and stability of the branch-site recognition region, which is necessary for pre-mRNA splicing (8–10). Because of the prevalence of Ψ s in structured RNAs, we investigated whether Ψ s were present in the RNA subunit of human telomerase (hTER). Here, we report the first evidence of potential Ψ modifications in hTER, and the effect of pseudouridylation in the hTER P6.1 hairpin on its structure and stability and on its function in telomerase catalytic activation.

Telomerase is a unique ribonucleoprotein (RNP) enzyme complex that maintains telomeres by adding telomeric DNA repeats at the ends of chromosomes using its intrinsic RNA template (11–15). The minimal components of the telomerase RNP for *in vitro* catalytic activity are the catalytic protein subunit, telomerase reverse transcriptase (TERT), which provides the active site for deoxyribonucleotide addition, and the telomerase RNA (TER), which provides the template sequence for TERT (14). TER interacts with TERT and with other

*To whom correspondence should be addressed. Tel: +1 310 206 6922; Fax: +1 310 825 0982; Email: feigon@mbi.ucla.edu
Present addresses:

Carla A. Theimer, Department of Chemistry, State University of New York, Albany, NY 12222, USA.

James R. Mitchell, Department of Genetics and Complex Diseases, Harvard School of Public Health, Boston, MA 20115, USA.

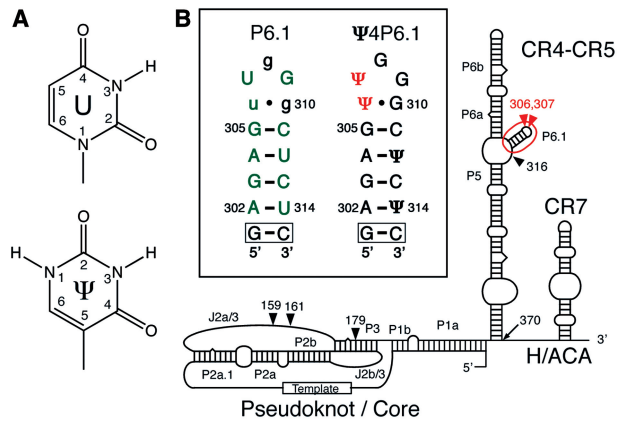


Figure 1. Secondary structure of hTER and structure of Ψ. (A) Comparison of the structures of uridine and Ψ. (B) Secondary structure of the unmodified P6.1 (left) and Ψ modified (right) domains. Right: the naturally occurring Ψ modification sites are shown in red and two Ψs in the stem substituted during *in vitro* RNA synthesis in bold black. Left: upper case green, lower case green and black residues stand for 100%, $\geq 80\%$ and $< 80\%$ conserved nucleotides in vertebrate TER, respectively. In both P6.1 and Ψ4-P6.1, the terminal G-C pairs (box) are not from the natural hTER sequence. Secondary structures of hTER showing the pseudoknot/core, CR4-CR5, CR7 and H/ACA domains. Putative Ψ modification sites are indicated by arrows, with the P6.1 sub-domain circled in red.

telomerase-associated proteins that are essential for telomerase function *in vivo* (12,14,16). TER secondary structure includes motifs required for catalytic activity and species-specific sub-domains that play critical roles in telomerase function and assembly (15,17–19). The 451 nt hTER (Figure 1B) and other vertebrate TERs have two regions required for catalysis, the pseudoknot/core and a conserved region (CR) domain CR4-CR5, and other regions required for cellular localization, TER accumulation and TER 3'-end processing (17). The pseudoknot/core domain, located in the 5'-half of hTER, has a large pseudoknot, which contains a phylogenetically conserved and catalytically important triplex structure (20,21), as well as an hTERT binding site, the template and a template boundary element (17,22,23). The CR4-CR5 domain is required for telomerase activity and includes a TERT binding site in the P6.1 sub-domain and a large internal loop (24,25). The 3'-half of hTER, excluding the CR4-CR5 region, folds as an H/ACA RNA domain and binds the H/ACA RNP proteins GAR1, NHP2, dyskerin and NOP10. The H/ACA domain of hTER is important *in vivo* for hTER accumulation, 3'-end processing and localization (26–28). The CR7 region of the H/ACA domain has been shown to be important for Cajal body localization through the CAB box in its terminal loop (28,29).

The pseudoknot/core and CR4-CR5 domains combined *in cis* or *trans* are necessary and sufficient for reconstitution of telomerase activity *in vitro* (30). Within the CR4-CR5 domain, the P6.1 hairpin has been shown by mutational studies of hTER and mouse TER to be required for telomerase activity and TERT binding (22,24,25,31). Base pairing in the P6.1 stem has been shown to be critical for TERT binding and telomerase activity, although the sequence of the stem is not critical

(24,25). The NMR solution structure of the P6.1 stem-loop revealed an A-form duplex capped with a U•G wobble pair and three solvent-exposed loop bases (32). Two of these three loop nucleotide bases are well conserved and critical for activity of telomerase RNP reconstituted *in vivo*, although none of them are required for hTER-TERT interaction (25).

In this study, we first identified up to six potential sites of Ψ modification in hTER. Two of them are of particular interest, as they are located in the loop of P6.1 essential for telomerase activity. We therefore investigated the influence of Ψ substitutions on P6.1 structure, thermodynamic stability and telomerase enzymatic activity. We determined the NMR solution structure of the pseudouridylated P6.1 hairpin. Direct comparison with P6.1 revealed that the presence of the Ψs resulted in a significant change in the positions of all of the loop nucleotides including the helix-capping U•G base pair. Thermal denaturation studies revealed that the Ψs in the loop substantially stabilize the P6.1 RNA hairpin fold. Direct telomerase activity assays of *in vitro* reconstituted enzyme showed that the pseudouridylated P6.1 sequence slightly attenuated telomerase activity and slightly increased processivity, indicating that Ψ modification has a subtle effect on telomerase enzyme properties.

MATERIALS AND METHODS

Identification of potential sites of Ψ modification

To avoid possible artifacts from altered expression level or expression context, we used endogenous hTER to map potential sites of post-transcriptional modification. However, the low level of endogenous hTER introduced a technical challenge for detection. To detect the extension of a radio-labeled primer templated by endogenous hTER, telomerase partial purification was required prior to RNA isolation. We enriched active telomerase from HeLa S-100 extract by binding to phosphocellulose under relatively stringent conditions (0.4 M KCl in buffer with 20 mM HEPES-KOH, 2 mM MgCl₂, 0.2 mM EGTA, 2 mM DTT and 20% glycerol at pH 8) and eluting with a step to doubled salt concentration. Enrichment of hTER was verified by blot hybridization. RNA purified from the enriched fraction was split for parallel primer extension reactions of template without any additional handling (E) or treated with *N*-cyclohexyl-*N'*-β-(4-methylmorpholinium) ethylcarbodiimide *p*-tosylate, CMC (+) or mock-treated under the same conditions as the CMC reactions but without CMC (-). CMC modification and reverse transcription (RT) were done according to standard methods, with the same conditions used in earlier studies (33). Two 5' ³²P-end-labeled DNA oligonucleotides complementary to nucleotides 443–419 or 235–211 of mature hTER were used for primer extension. In addition to the endogenous RNA samples for primer extension, a sequencing ladder of ddNTP chain termination was generated using recombinant template (33,34). CMC-dependent terminations of RT that occur one nucleotide before a uridine are potential sites of Ψ modification.

RNA synthesis and purification

For NMR studies, unlabeled and ^{13}C , ^{15}N -A,C,G-labeled Ψ 4-P6.1 RNA (5'-GAGAG Ψ Ψ GGGC Ψ C Ψ C-3'), and unlabeled P6.1 (5'-GAGAGUUGGGCUCUC-3') (Figure 1) were prepared by *in vitro* transcription using T7 RNA polymerase (P266L mutant) (35) with synthetic DNA templates. The Ψ -5'-triphosphate was purchased from Trilink Biotechnologies. In both Ψ 4-P6.1 and P6.1 RNAs, the terminal nucleotides G and C were added for efficient transcription. The transcribed RNA was ethanol precipitated, purified using 20% (19:1 cross-linking ratio) denaturing PAGE, electroeluted (Elutrap, Whatman) and further purified by anion-exchange on a 5-ml Hi-Trap Q column (GE Healthcare). All purified RNAs were desalted and exchanged extensively into water using the Amicon filtration system (Millipore). The RNA samples were heated to 95°C under dilute (1–10 μM RNA) conditions for 5 min, snap-cooled on ice for 30 min, concentrated to $\sim 0.8\text{ mM}$ and the pH was adjusted to 6.8 with KOH. The final concentration of added K^+ was $\sim 5\text{ mM}$. At higher salt concentrations the sample converts from hairpin to dimer during the time required to collect NMR data (15-bp duplexes were formed, identified in 1D and 2D imino NOESY spectra, Supplementary Figure S1 and data not shown). Even under these low-added salt conditions, the NMR samples would begin to dimerize when stored at 20°C for >1 day, so the samples needed to be re-annealed before and checked for dimerization after each NMR experiment (Supplementary Figure S1).

For telomerase activity studies, the hTER RNAs, full length (nucleotides 1–451) and CR4-CR5 domain (nucleotides 243–326), were transcribed *in vitro* using linearized DNA template obtained from PCR amplification of the pBShTER plasmid using the forward and reverse strand primers. The T7-MEGAShortsript kit (Ambion) was used for transcription of full length and CR4-CR5 RNA constructs. RNA products were gel purified (4% 19:1 denaturing PAGE), eluted in $0.5\times$ TAE using the Centrilter system (Millipore) and concentrated. The truncated CR4-CR5 construct, CR5318 (nucleotides 253–318, where nucleotides 271–285 were replaced with a GAAA tetraloop) was transcribed *in vitro* using T7 RNA polymerase with a synthetic DNA template as described earlier. The Ψ 3CR5318 and Ψ 2CR5318 (CR5318 with Ψ modifications at three nucleotides 306, 307 and 316, and with two nucleotides 306 and 307, respectively) and the two Ψ -modified P6.1 constructs, Ψ 2L-P6.1 (5'-GAGAG Ψ Ψ GGGCUCUC-3') and Ψ 2S-P6.1 (5'-GAGAGUUGGGC Ψ C Ψ C-3'), were purchased from Dharmacon (Thermo Fisher Scientific Inc.) and purified using 15% (19:1) denaturing PAGE. The hTER pseudoknot/core domain (nucleotides 34–191) includes three extra G-C base pairs at the P1b terminus to stabilize the helix (CGG and GCC at the 5'- and 3'-ends, respectively). A linearized PCR-amplified DNA including EcoR1 (5'-end) and Nco1 (3'-end) restriction sites was produced using the pBShTER plasmid and primers, and ligated into pre-digested (EcoR1/Nco1) pUC19 with the HDV ribozyme sequence at the 3'-end

in order to obtain homogenous 3'-termini. The plasmid DNA was prepared using the Giga kit (Qiagen) and linearized with BamH1 (Invitrogen). The restriction site is located at the 3'-end of the HDV ribozyme. The pseudoknot/core domain RNA was generated by HDV ribozyme cleavage during *in vitro* transcription using T7 polymerase, and purified as described earlier.

NMR spectroscopy and structure calculations

NMR spectra were recorded on Bruker DRX or Avance 500, 600 and 800 MHz spectrometers equipped with HCN cryoprobes or QXI probe. For the peak assignments, exchangeable proton spectra were taken in 95% $\text{H}_2\text{O}/5\%$ D_2O at 283 K and non-exchangeable proton spectra in 99.996% D_2O (Sigma) at 293 K. NMR spectra were processed and analyzed using XWINNMR 3.5 (Bruker) and Sparky 3.110. (University of California, San Francisco, CA, USA.) The standard H1'-base proton sequential assignments were initially obtained from analysis of 2D NOESY and 2D TOCSY experiments on unlabeled RNA samples. The assignments for all non-exchangeable protons were achieved from analysis of 2D NOESY, 2D ^1H - ^{13}C HSQC, 2D HCCH-COSY and 3D HCCH-TOCSY (36,37). A suite of 2D-filtered/edited proton NOESY (F2f, F1fF2e, F1fF2f and F1eF2e) experiments on ^{13}C , ^{15}N -A,C,G-labeled Ψ 4-P6.1 RNA were used to resolve ambiguous assignments in overlapped regions and obtain NOE restraints, as previously described (38). The imino and amino exchangeable protons were assigned from 2D NOESY, 2D ^{15}N -correlated CPMG NOESY and 2D ^1H - ^{15}N HMQC spectra acquired on samples in 95% $\text{H}_2\text{O}/5\%$ D_2O . The 2'-hydroxyl protons were identified by scalar coupling to H2' protons observed in 2D DIPSI TOCSY ($\tau_m = 43\text{ ms}$) (39) and by NOE correlation with H1's observed using 2D flip-back water gate NOESY ($\tau_m = 50\text{ ms}$) (40,41; Supplementary Figure S2) Residual dipolar couplings (RDCs) for Ψ 4-P6.1 RNA were measured from the differences in the splitting in the ^1H dimension of HSQC spectra (42) (800 MHz), in the absence and presence of Pf1 phage (16 mg/ml, ASLA Biotech, Ltd).

Interproton distances were generated from the 2D NOESY spectrum ($\tau_m = 100\text{ ms}$) as well as 2D-filtered/edited NOESY spectra (38). NOE distance restraints were classified as strong (1.8–3.5Å), medium (1.8–4.5Å), weak (1.8–5.5Å) and very weak (1.8–6.5Å). A total of 137 intra-nucleotide and 136 inter-nucleotide NOE derived distance restraints and 88 dihedral angle restraints (α , β , γ , δ , ϵ , χ , ν_2 and ζ) were used in the structure calculations, where the δ , ϵ and χ were determined experimentally as described below. The α , β , γ , ν_2 and ζ dihedral angles for the nucleotides involved in base pairs in the helix were constrained to the A-form values ($-62.1 \pm 30^\circ$, $180.1 \pm 30^\circ$, $47.4 \pm 30^\circ$, $37.3 \pm 30^\circ$ and $-74.7 \pm 30^\circ$, respectively). $^3\text{J}_{\text{H}_2\text{P}}$ and $^3\text{J}_{\text{CP}}$ were measured using ^{31}P spin echo difference CT HSQCs to determine the ϵ dihedral angles for the loop residues (43). Final structure calculations included hydrogen bond distance restraints for the five Watson-Crick base pairs, and a non-Watson-Crick base pair as previously

described (44). Weak base pair planarity and hydrogen bonding restraints were used for unambiguously assigned base pairs. Nucleotide G309, which showed a strong intra-nucleotide H1'-aromatic NOE and a weak intra-nucleotide H2'-aromatic NOE in a 2D NOESY ($\tau_m = 50$ ms), was restrained to the *syn* glycosidic torsional angle ($\chi = 60 \pm 30^\circ$), while all other nucleotides were restrained to 'anti' ($\chi = -160 \pm 30^\circ$). The ribose conformation was constrained to C2'-*endo* ($\delta = 145 \pm 30^\circ$) for residues G308 and G309, based on a strong NOE cross peak between the H1' and H2' protons and observable H1'-H3' couplings in a 50-ms mixing time 2D TOCSY spectrum (45). A total of 27 one bond C-H RDCs ($^1D_{C1'H1'}$, $^1D_{C8'H8}$, $^1D_{C6'H6}$, $^1D_{C5'H5}$ and $^1D_{C2'H2}$) were obtained. One hundred initial structures of Ψ 4-P6.1 were calculated using XPLOR-NIH 2.9.8 starting from an extended, unfolded RNA using the NOE distance and dihedral angle restraints following standard XPLOR protocols. The 25 lowest energy structures were further refined by inclusion of RDCs for the final structures. Experimental restraints and structural statistics for the 20 lowest energy structures are shown in Table 1. All structures were viewed and analyzed using MOLMOL (46) and PYMOL (DeLano Scientific LLC).

Thermal denaturation

Thermal melting experiments were performed on a Beckman DU800 spectrophotometer equipped with a Peltier heating block accessory. Three micro molar RNA samples were prepared in 5-mM MOPS buffer (pH 6.8) without any additional salt, consistent with the NMR solution conditions. The temperature was increased at a rate of 0.3°C/min from 10 to 95°C, with data collected at 0.3°C increments at both 260 and 280 nm. Melting profiles

were obtained by taking the first derivative of the absorbance with respect to temperature ($\partial A/\partial T$) and subjected to non-linear least-squares parameter estimation of $t_{m,i}$ (melting temperature), ΔH_i (van't Hoff enthalpy), A_i^{260} and A_i^{280} ($\partial A/\partial T$ amplitude at 260 and 280 nm) for each *i*th transition upon application of a sequential two-state unfolding model using the *tmelt* program (Supplementary Figure S3) (47).

In vitro reconstitution and direct telomerase activity assay

N-terminally S-tagged hTERT in pCITE4a was expressed using the TNT quick-coupled transcription/translation rabbit reticulocyte lysate (RRL) system (Promega) according to the manufacturer's instruction. Briefly, hTERT protein was translated in 10 μ l of RRL for 1 h at 30°C. *In vitro* synthesized TER with a final concentration of 1 μ M was added, and telomerase RNP was reconstituted by incubating the mixture for 30 min at 30°C. *In vitro* telomerase activity was monitored using the direct telomere extension assay. For telomere extension reactions, 3 μ l of the reconstituted telomerase RNP was added to a total of 10 μ l of reaction mix which includes 1 \times PE buffer (50 mM Tris-HCl (pH 8.0), 50 mM KCl, 2 mM DTT, 3 mM MgCl₂, 1 mM spermidine), 1 mM dATP, 1 mM dTTP, 2 μ M dGTP, 0.25 μ l of 32 P- α -dGTP (3000 Ci/mmol) and 1 μ M DNA primer (T₂AG₃)₃. The reaction mixture was incubated for 1 h at 30°C in a heat block. A 32 P 5'-end labeled 15-nt DNA loading control was added, and the telomeric DNA products were extracted by using phenol-chloroform-isoamyl alcohol (pH 7.9), and ethanol precipitated for 1 h at -80°C. The products were resolved by gel electrophoresis on a 10% denaturing gel (19:1 cross-linking ratio) in 1 \times TBE buffer. Gels were dried, and products were detected and analyzed using a phosphorimager (BioRad FX Pro). The activity was determined by measuring the total intensity of extended telomere primers after background correction and normalizing against the loading control (48).

Table 1. NMR restraints and statistics for the Ψ 4-P6.1

NOE distance and dihedral constraints	
Distance restraints	
Total NOEs	273
Intra-residue	137
Inter-residue	136
Hydrogen bonds	27
Base-pair planarity restraints	6
Total dihedral angle restraints	88
Total RDC restraints ($^1D_{CH}$)	27
Structure statistics	
Deviation from idealized geometry (20 structures)	
Distance restraints (Å)	0.016 \pm 0.001
Dihedral angle restraints (°)	0.030 \pm 0.014
Bond lengths (Å)	0.005 \pm 0.0001
Bond angles (°)	1.043 \pm 0.003
Improper (°)	0.379 \pm 0.005
Dipolar couplings (Hz)	0.62 \pm 0.04
Violations	
Number of NOE violations >0.2 (Å)	0
Number of NOE violations >0.5 (Å)	0
Number of Dihedral violations >5 (°)	0
Number of RDC violations >2 (Hz)	0
Average r.m.s.d. (Å) from the mean structure for 20 lowest energy structures (all heavy atoms)	
All residues	0.68 \pm 0.12
Stem including Ψ 306-G310 pair	0.51 \pm 0.11
Loop (residues 307-309)	0.74 \pm 0.20

RESULTS AND DISCUSSION

Identification of candidate sites of pseudouridylation in hTER

In order to identify potential sites of pseudouridylation in hTER, we performed chemical modification and RT of endogenous hTER from partially purified HeLa cell extract ('Materials and Methods' section). Irreversible CMC modification of Ψ forces a halt of RT 1 nt before the modified base (34). Across the nearly full length of hTER, excluding the 3'-region impossible to examine by extension of an annealed primer, we identified a maximum of six possible pseudouridylation sites. Due to the low level of endogenous hTER template, long exposures of the radio-labeled primer extension products were required to detect CMC-dependent stops of RT (Figure 2). It is important to note that the mapping of modification sites by RT does not indicate the stoichiometry of a modification or the number of modifications present simultaneously in a given hTER molecule, nor does it directly demonstrate the presence of a modified

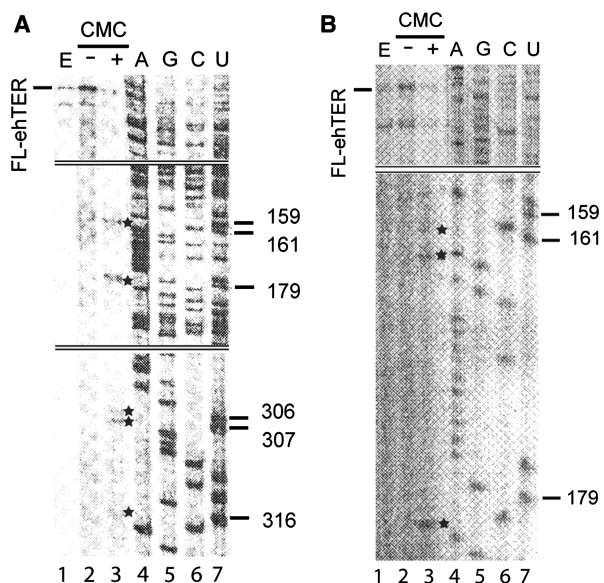


Figure 2. Identification of Ψ modification sites in hTER. Ψ s were detected as stops to primer extension on modified RNA from a HeLa extract fraction enriched for endogenous hTER. Lane 1: untreated RNA as template; lanes 2 and 3: CMC mock-treated or CMC-treated RNA as template. The stops to RT that occur one nucleotide before potential sites of Ψ modification are marked with asterisks. Lanes 4–7: RT of recombinant template was performed with ddNTP mixes to generate a sequencing ladder. The non-specific background pattern is an artifact of scanning a long radiographic exposure at high gain, which was required to visualize the weak signals. The RT product of complete synthesis to the hTER 5'-end is indicated (FL-ehTER). (A) Primer extension using primer complementary to hTER nucleotides 443–419. (B) Primer extension using primer complementary to hTER nucleotides 235–211.

base. However, Ψ is the only known base modification that imposes a CMC-dependent block to RT. In each assay repetition one candidate site of Ψ modification (nt 316) was relatively weakly detected as a CMC-dependent RT stop and two candidate sites (nucleotides 159 and 161) were located within a sequence-variable region of hTER that is not essential for catalytic activity (49). An additional candidate site of Ψ modification was within the base paired P3 stem of the pseudoknot (nt 179). Ψ modification would not be likely to change the structure of this hTER region (20,44), although the additional hydrogen bonding capability provided by the N1H imino proton and enhanced base stacking could increase stem pairing stability as shown for other RNA helices (5,6,9,10,50–54) and discussed in the context of P6.1 below. The remaining two potential modification sites, P6.1 nucleotides 306 and 307, are of interest due to their high-sequence conservation and critical function in telomerase catalytic activation. Positions of Ψ s in other non-coding RNAs such as tRNA, rRNA and snRNAs are thought to be efficiently modified, so it is likely that most modifications of hTER would affect the bulk of the RNA population as well.

The P6.1 hairpin (Figure 1B) has a conserved stem (nucleotides 302–305 and nucleotides 311–314) with strikingly highly conserved sequence, despite the ability of altered stem sequences to support catalytic activity of telomerase

RNPs reconstituted *in vitro* or *in vivo* (24,25). In the loop (nucleotides 306–310), U306 is 83% conserved and U307 is 100% conserved across vertebrate TERs (55). Among the other loop nucleotides, G309 is also absolutely conserved, but G308 and G310 are not conserved. Disruption of the P6.1 stem base pairing inhibits TERT binding (22,24,25). Substitutions of the conserved loop nucleotides U307 and G309 inhibited telomerase catalytic activity without inhibition of TERT binding, while substitution of the intervening non-conserved G308 did not have a major impact on TERT binding or enzyme activity (24,25). The identification of potential Ψ modifications of P6.1 loop nucleotides 306 and 307 led us to investigate the effect that these modified nucleotides would have on P6.1 structure and function in telomerase activation.

NMR spectroscopy of pseudouridylated P6.1

For NMR structural studies, we used a 15-nt Ψ 4-P6.1 RNA that includes all of the conserved nucleotides in the stem and the loop (Figure 1B, right), but all four uridines in the RNA were substituted with Ψ s. This allowed us to incorporate Ψ within a ^{13}C , ^{15}N -A,C,G-labeled RNA prepared by *in vitro* transcription with T7 RNA polymerase. As discussed below, the Ψ s in the stem do not disrupt the A-form helix or affect the loop conformation. One G-C base pair was added to the terminus of the stem for transcription efficiency.

All of the expected imino protons from the Ψ 4-P6.1 hairpin stem including the characteristic N1H protons from Ψ s are present in the imino proton spectra (Figure 3A), and were assigned from NOESY spectra. The imino proton of G310 resonates at 11.7 p.p.m., which is upfield shifted compared to Watson-Crick base pair hydrogen bonding, and has a weak imino to imino cross peak with G305. The identities of the N1H protons of all four Ψ s in the Ψ 4-P6.1 were confirmed based on cross peaks with their own H6 protons. The N3H protons of Ψ s in the stem were identified by strong NOESY cross peaks with the AH2 protons of their Watson-Crick base pairs. At longer mixing times, intra-base NOE cross peaks between the Ψ N3H and Ψ N1H appeared in the 2D NOESY spectrum through spin diffusion (Figure 3A). The N3H protons of Ψ 306 and Ψ 307 were not visible, indicating that they are not protected from exchange with water.

The base- H1' region of the Ψ 4-P6.1 2D NOESY spectrum was well dispersed, and also showed the characteristic upfield shifted H1' resonances of Ψ s (Figure 3B, black). Nearly complete assignments were obtained using unlabeled and ^{13}C , ^{15}N -A,C,G-labeled samples as described in 'Materials and Methods' section.

Solution structure of the Ψ 4-P6.1

The structure determination of Ψ 4-P6.1 included 273 NOE distance restraints for an average of 18 NOE restraints per nucleotide (Table 1). Ψ 4-P6.1 has a well-defined structure with an RMSD to the mean of $0.68 \pm 0.12 \text{ \AA}$ for all heavy atoms for the 20 lowest energy structures (Figure 4A). The Ψ 4-P6.1 structure has

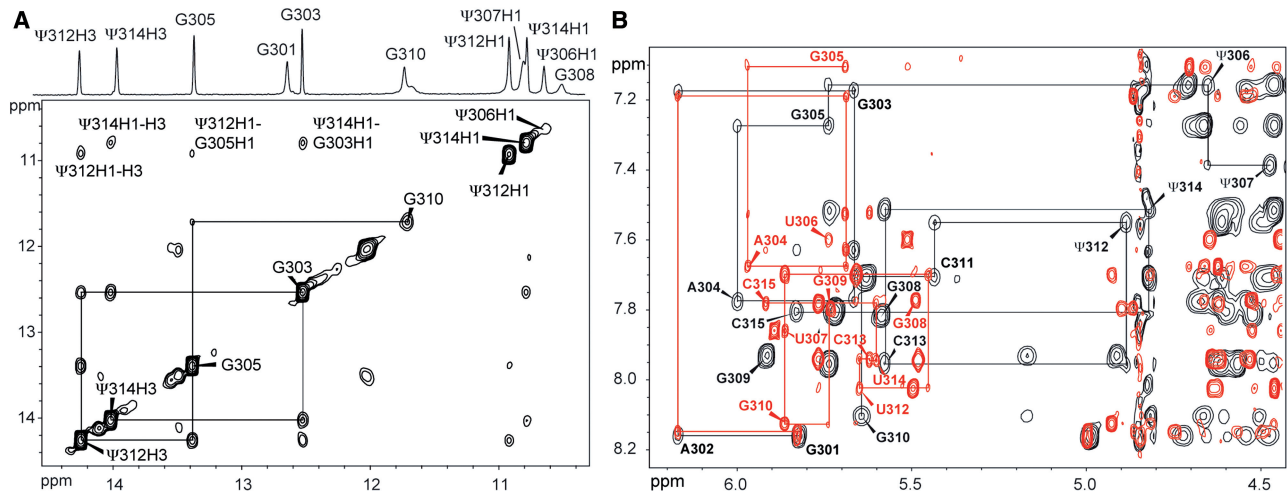


Figure 3. NMR spectra of Ψ 4-P6.1 and comparison with P6.1. (A) 1D imino (600 MHz, 10°C) and 2D NOESY (600 MHz, 10°C, $\tau_m = 250$ ms) spectra of Ψ 4-P6.1. (B) Comparison of NOESY spectra of Ψ 4-P6.1 (black, 600 MHz, $\tau_m = 200$ ms) and P6.1 (red, 800 MHz, $\tau_m = 150$ ms) at 20°C. Large chemical shift differences are observed for the residues 305, 308, 309 and 310 as well as between Ψ s and Us.

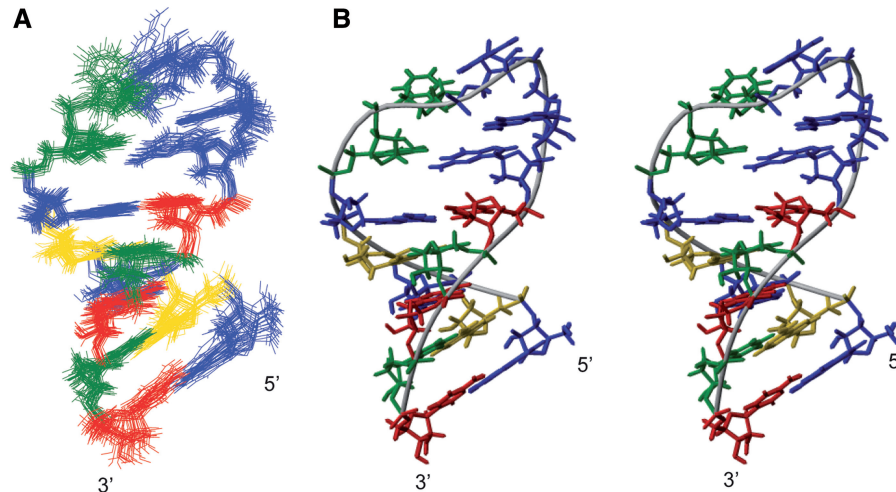


Figure 4. NMR solution structure of pseudouridylated P6.1 (Ψ 4-P6.1). (A) Superposition of the 20 lowest energy structures over all heavy atoms. (B) Stereo view of the lowest energy structure of Ψ 4-P6.1. Phosphate backbone is outlined by a gray ribbon. In both (A) and (B), nucleotides A, Ψ , G and C are colored by yellow, green, blue and red, respectively.

a stem that forms a standard A-form helix capped by a Ψ 306•G310 base pair from the loop (Figure 4B). The loop is highly structured except for the non-conserved and functionally non-critical G308, which had few inter-residue NOE restraints. The Ψ 306•G310 base pair is formed by the first and last nucleotide in the loop stacking on the stem, and has a single hydrogen bond between the imino proton of G310 and the C4 carbonyl oxygen of Ψ 306, where N3H of Ψ 306 is exposed to solvent exchange (Figures 4B and 5A). In the structure calculations, the G310 N1H was consistently within hydrogen bonding distance to Ψ 306 O4. The alternative possibility that G310 N1H could be hydrogen bonded to Ψ 306 2'O was excluded, since no NOEs were detected between the ribose 2'OH and G310 N1H in a water NOESY spectrum (39,40). On the 5'-side of the loop Ψ 306 and Ψ 307 are stacked on G305 and Ψ 306, respectively (Figure 4B).

Consistent with this, aromatic to H1' sequential NOE connectivities characteristic of right-handed helices were observed from G305 to Ψ 307 (Figure 3B, black). Note that the chemical shifts of the H1' protons of Ψ s appear upfield of those of A, U, C and G, due to the absence of N1 nitrogen in the Ψ base. Both Ψ 306 and Ψ 307 are in the major groove of the RNA, with their respective N1H protons positioned within water-mediated hydrogen bond distance of their respective 5'-phosphate oxygen atoms. The base of the non-conserved G308 is flipped out of the loop on the minor groove side. In the 3'-half of the loop G310 is stacked on C311 at the top of the stem. The turn in the phosphodiester backbone occurs between G308 and G309. G308 has a 2'-endo sugar pucker, which allows the loop nucleotides to span the width of the helix, and G309 is in the *syn* conformation to stack on the sugar of G310.

The pseudouridylated P6.1 loop adopts a different conformation than that of unmodified P6.1

While the total number of constraints used for structural calculations of Ψ 4-P6.1 (421 restraints) and unmodified P6.1 (395 restraints) are comparable, (Table 1; 32), comparison of the structure of Ψ 4-P6.1 and unmodified P6.1 (PDB 1OQ0) (32) revealed significant differences in the structures of the loops including the helix capping U•G (or Ψ •G) base pairs (Figure 5). Consistent with this, significant chemical shift differences are observed for the H8' and H1' resonances of G305, G308, G309 and G310 (Figure 3B; Supplementary Figure S4; discussed below). In the unmodified P6.1, all of the unpaired loop nucleotides, U307, G308 and G309, are exposed to solvent. The bases of U307 and G309 point out into solution on the minor groove side of the loop, and the base of G308 is partially stacked on U306 on the major groove side of the loop. The backbone turns after U307, and the phosphodiester backbone is extended between G308 and G309 (Figure 5B). In contrast, in Ψ 4-P6.1 the base of Ψ 307 is stacked over Ψ 306 in the major groove of the loop to maintain A-form helical stacking on the 5'-side of the loop. The non-conserved G308 is pointing out into the minor groove and is the only solvent exposed loop nucleotide in Ψ 4-P6.1, the backbone turns after G308 rather than G307, and G309 is stacked on the G310 sugar. The wobble pairs Ψ 306•G310 and U306•G310 are similar in location in Ψ 4-P6.1 and P6.1, respectively, but Ψ 4-P6.1 has only one hydrogen bond between the N1H of G310 and O4 of Ψ 306, while P6.1 has a canonical U•G wobble pair, which consists of two hydrogen bonds between pairs of imino protons and carbonyl oxygen atoms (Figure 5C and D).

Both of these wobble pairs are different from the base pair observed in the UUCG tetraloop (56,57), where the G nucleotide is in the *syn* conformation and its N1H and O6 hydrogen bonds with the O2 and 2'-OH of the 5'-U nucleotide (Figure 5E). The G310 amino is too far away from the Ψ 306 2'-oxygen to form a hydrogen bond in Ψ 4-P6.1, and consistent with this, no NOEs were detected between the Ψ 306 2'OH and the G310 amino or imino protons.

In order to confirm that the differences in the P6.1 loop structures were due to the presence of the Ψ 306 and Ψ 307, and not differences in sample conditions, we obtained 1D and 2D NOESY spectra of unmodified P6.1 under the same solution conditions as Ψ 4-P6.1. We compared chemical shifts, NOE patterns and NOE intensities between the Ψ -modified and unmodified P6.1 and between our P6.1 sample and the one used for the previously reported structure of the unmodified P6.1 RNA hairpin (32). The observed chemical shifts, NOE patterns and intensities for our P6.1 sample are the same, within experimental error, as those reported for 1OQ0. For Ψ 4-P6.1 and P6.1, the chemical shifts for the base and H1' protons are similar for the stem residues of G301, A302, G303, C311 and C313, but there are key differences in NOE patterns and intensities for the loops of P6.1 and Ψ 4-P6.1 (Figure 3B) that are not due to the difference in chemical structure between U and Ψ . For example, NOEs for U306 H2'-G308 H8 (medium), U306 H1'-G308 H5' and H5'' (weak) are only observed in P6.1, indicating that the G308 base is close to U306, whereas NOEs between G308 H3'-G309 H2' and G308 H3'-G309 H3' are only found in the Ψ 4-P6.1 spectra. In Ψ 4-P6.1, a

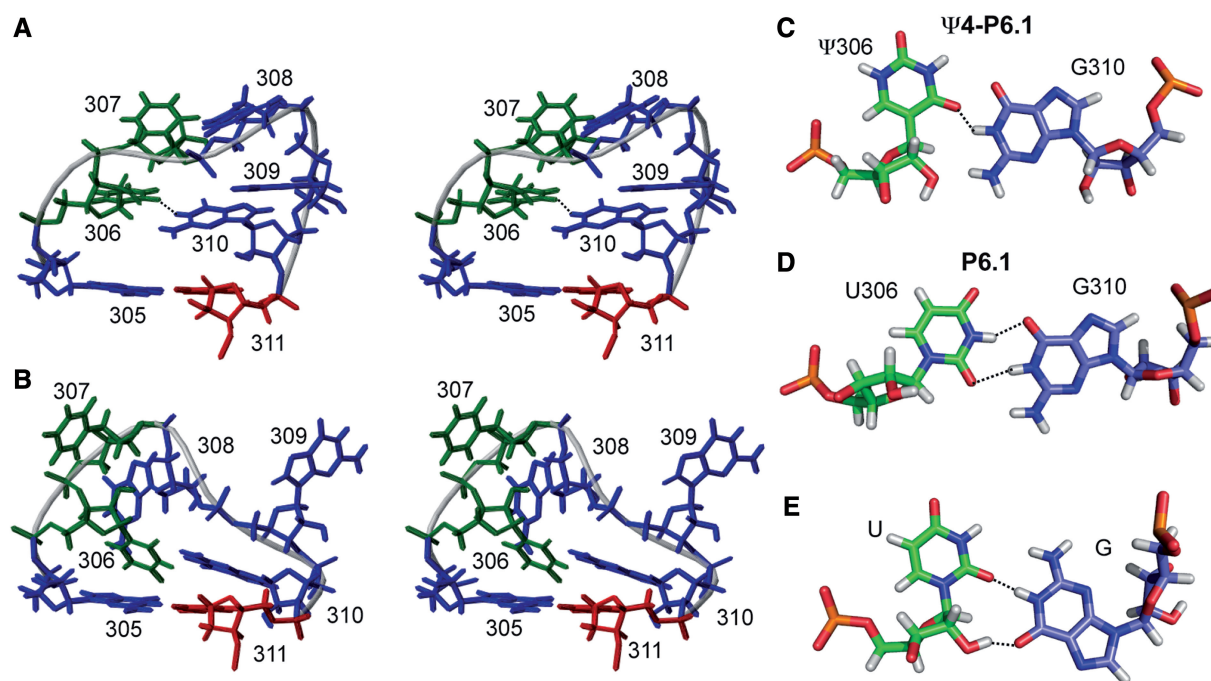


Figure 5. Detailed tertiary structure of the loop regions of Ψ 4-P6.1 and P6.1. Stereo view of the loop from the lowest energy structure of (A) Ψ 4-P6.1 and (B) P6.1 [PDB ID: 1OQ0; (32)]. Nucleotides are color-coded as shown in Figure 2B. Comparison of U•G wobble pairs in (C) Ψ 4-P6.1, (D) P6.1 and (E) the UUCG tetraloop [PDB ID: 1F7Y; (56)].

strong NOE for Ψ 307 H6- Ψ 306 H2' restrains Ψ 307 in an A-form helical stack on top of Ψ 306 (Figure 5A), while the corresponding NOE for P6.1 is observed to be weak.

Effect of pseudouridylation in P6.1 on RNA stability

Pseudouridine modifications usually increase the stability of an RNA duplex region by forming water-mediated hydrogen bonds between Ψ N1H protons and the 5'-neighboring phosphate, as well as by enhancing base stacking interactions (5,8,53,54). In order to investigate the effect of pseudouridylation on P6.1 thermal stability, we performed thermal denaturation experiments for four different P6.1 constructs: the unmodified P6.1 and the fully modified Ψ 4-P6.1, for direct comparison of the stability between unmodified P6.1 and the construct that we used for NMR structural studies, Ψ 2L-P6.1 (P6.1 with two Ψ s in the loop at positions 306 and 307) and Ψ 2S-P6.1 (P6.1 with two Ψ s in the stem at positions 312 and 314), as controls to identify the dependence of the stability on the location of the Ψ s in the P6.1 structure (Table 2; Supplementary Figure S3). In all cases, insertion of a Ψ in place of a U in the P6.1 sequence (in the loop or in the stem), increased the observed melting temperature and enthalpy of the unfolding transition, resulting in an increase in the calculated stability, ΔG_{37} . Ψ 4-P6.1 is the most stable ($\Delta G_{37} = -3.1 \pm 0.4$ kcal/mol) of the four RNAs, with a melting temperature (T_m) of $\sim 61^\circ\text{C}$, which is ~ 1.6 kcal/mole and 12 degrees greater than the ΔG_{37} and T_m , respectively, of the unmodified P6.1. Both Ψ 2L-P6.1 and Ψ 2S-P6.1 are intermediate in T_m and stability between the fully modified and unmodified P6.1 RNAs, with Ψ 2L-P6.1 more stable than Ψ 2S-P6.1. Thus, while the Ψ s in the stem do increase the RNA stability as expected, this effect is not as dramatic as Ψ substitution in the loop. The $\Delta\Delta G$ values show that the stability of the Ψ 4-P6.1 is, within experimental error, the summation of the stabilizing effects observed in the stem- and loop-only Ψ substituted RNAs, Ψ 2L-P6.1 and Ψ 2S-P6.1, respectively. Notably, the enhanced stability of the Ψ 4-P6.1 is due predominantly to the enhanced stability in the loop. Thus, the presence of Ψ s at positions 306 and 307 of hTER would be expected to stabilize the P6.1 helix in its native context in the CR4-CR5 domain. This increased stabilization in the pseudouridylated P6.1 loop can be attributed to the additional stacking interactions between Ψ 307 and Ψ 306, which are not present in the P6.1 structure, and potential water mediated hydrogen bonds between N1H protons on Ψ 306 and Ψ 307 and their respective 5'-phosphates, observed in the solution

structure of Ψ 4-P6.1. The Ψ modification of U307 has a greater effect on the stability of the RNA than U306, since as seen in the Ψ 4-P6.1 structure, Ψ 307 induces a large rearrangement of the loop structure compared to unmodified P6.1, while Ψ 306 only slightly affects the U•G base pair.

Effect of pseudouridylation in P6.1 on telomerase activity *in vitro*

hTER activity can be reconstituted *in vitro* with hTERT and the two catalytically essential sub-domains of hTER, the core and CR4-CR5 domains (22,30). In order to investigate the effect of the Ψ modification in the P6.1 subdomain on telomerase function, we performed direct telomerase activity assays *in vitro* using reconstituted telomerase RNP with the pseudoknot/core domain and two truncated CR4-CR5 constructs, CR5318 and Ψ 3CR5318, which include the catalytically essential P6a and P6.1 sequences (22,24) (Figure 6B). A two-component system was necessary since the CR4-CR5 fragment containing the Ψ s had to be chemically synthesized. Furthermore, using a two-component system reduces potential RNA folding heterogeneity. We tested the activity of telomerase RNP reconstituted with *in vitro* translated hTERT, the pseudoknot/core domain (nucleotides 34–191 with three G-C bps added at the P1b terminus) and full-length CR4-CR5 domain (nucleotides 243–326, CR4-CR5, versus the activity of RNP reconstituted with hTERT and full-length hTER (nucleotides 1–451, FL-hTER). Under our assay conditions, telomerase reconstitution with a separate pseudoknot/core domain and CR4-CR5 gave 3-fold greater activity than reconstitution with FL-hTER [Figure 6A (lanes 2 and 3) and C] with the same processivity (Figure 6D). This increased activity of telomerase assembled with separate core and CR4-CR5 domains was also reported previously and was attributed to the more heterogeneous folding potential of FL-hTER (30,58). CR5318 is a minimal CR4-CR5 construct in which the non-conserved nucleotides 271–285 were replaced with a GAAA tetraloop and most of the internal loop sequence was deleted except for the first three nucleotides before P6a and the 4nt after P6.1 (Figure 6B). Although the internal loop could potentially form additional base pairs (59), our direct telomerase activity assays indicate that base pairing of the internal loop is not required for activity (Figure 6A). This result is consistent with recent mutational studies of the CR4-CR5 domain, in which forcing various configurations of internal loop nucleotide pairing failed to

Table 2. Thermodynamic stabilities of the P6.1 constructs

Construct	T_m ($^\circ\text{C}$) ^a	ΔH (kcal/mole)	ΔG_{37} (kcal/mole)	$ \Delta\Delta G $ ^b (kcal/mole)
P6.1	49.1 ± 1.5	-40.1 ± 1.1	-1.5 ± 0.1	–
Ψ 4-P6.1	61.1 ± 2.1	-42.6 ± 1.3	-3.1 ± 0.4	1.6 ± 0.4
Ψ 2L-P6.1	57.3 ± 0.4	-44.5 ± 1.3	-2.7 ± 0.1	1.2 ± 0.2
Ψ 2S-P6.1	53.7 ± 0.7	-43.7 ± 0.4	-2.2 ± 0.1	0.7 ± 0.2

^a T_m was measured in 5-mM MOPS pH 6.8 without added salt. Experiments were performed in triplicate for error determination.

^b $|\Delta\Delta G|$ is the absolute value of the stability difference between unmodified P6.1 and the pseudouridylated P6.1 construct.

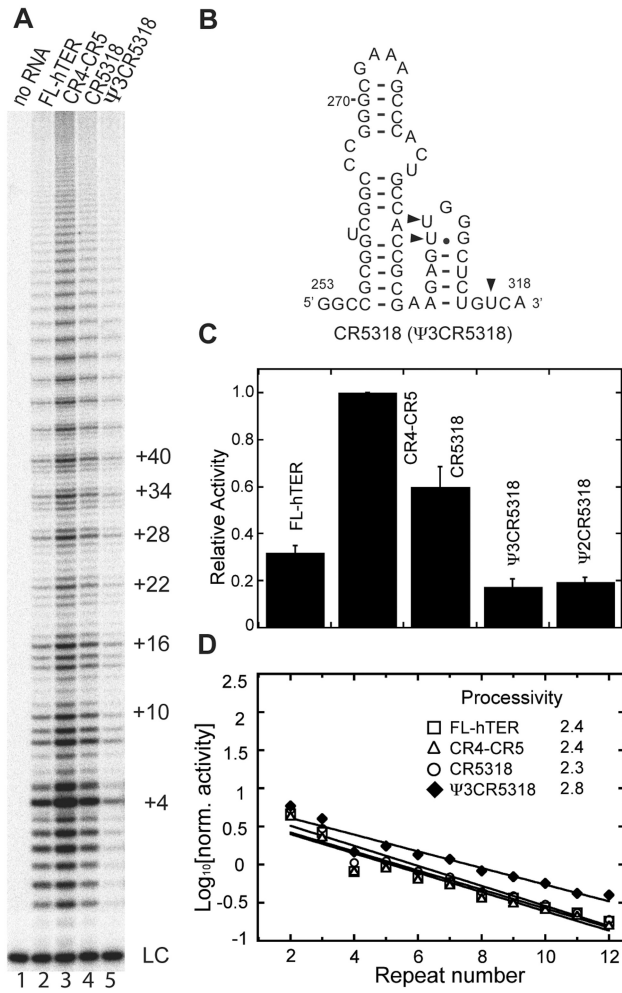


Figure 6. Direct telomerase activity assays of *in vitro* reconstituted telomerase with hTERT and hTER components. (A) Direct assays with FL-hTER (nucleotides 1–451), pseudoknot/core + CR4-CR5, pseudoknot/core + CR5318 and core + Ψ3CR5318 are shown from the lanes 2–5. Lane 1: mock reaction without RNA. The 15-nt ³²P-5'-end labeled DNA loading control (L.C.) is indicated. (B) The secondary structure of CR5318 with sites of Ψ modification marked with wedge symbols. Relative telomerase activities (C) and processivities (D) are shown for the RNAs listed in (A). The processivity = $-\ln 2 / (2.303k)$, where k is the slope of a linear fit (61).

support additional secondary structure formation as functionally significant (25). Comparing CR4-CR5 and the minimal CR5318 (Figure 6B), removal of P5 and most of the internal loop had a slight inhibitory impact on telomerase activity without impact on processivity (Figure 6A, C and D). We designed an RNA with Ψs at positions 306, 307 and 316, Ψ3CR5318 (Figure 6B). Direct telomerase activity assay results reveal that telomerase reconstituted with Ψ3CR5318 is ~3-fold less active than telomerase reconstituted with CR5318 but is slightly (~20%) more processive (Figure 6A, C and D). These differences are not due to misfolding of Ψ3CR5318, since both CR5318 and Ψ3CR5318 run at a similar rate as a single conformation on a non-denaturing polyacrylamide gel (Supplementary Figure S5). Nearly identical results in telomerase activity assays were obtained with

the RNA Ψ2CR5318 (Figure 6C), lacking the Ψ modification at nt 316 which was less definitively identified, indicating that the two Ψs in the P6.1 loop influence telomerase activity. Both the decrease in activity and the increase in processivity were reproducibly observed in assay repetitions.

CONCLUSIONS

Pseudouridine modifications in functional RNAs usually confer a selective advantage but are not required for activity (7,9). Thus, the modest extent of influence of Ψ modification of P6.1 loop nucleotides on telomerase activity *in vitro* is consistent with precedent. Our solution structure of pseudouridylated P6.1, when compared to the unmodified P6.1, revealed that the presence of Ψ306 and Ψ307 results in a significant rearrangement of the loop conformation including the positions of the highly conserved U306, U307 and G309 loop nucleotides. The U307 and G309 bases are flipped out and exposed to solvent on the minor groove side of the loop in unmodified P6.1 but are stacked on the stem-capping Ψ306-G310 base pair in Ψ4-P6.1. These nucleotides are stabilized in these positions by stacking interactions and additional water-mediated hydrogen bonding interactions between the Ψ306 and Ψ307 N1H and their respective 5'-phosphates, as revealed by the solution structure and thermal denaturation studies. The *syn* conformation of the G309 also places different hydrogen bond donors and acceptors in the minor groove. Thus, the conformation of the pseudouridylated P6.1 loop potentially provides a structural rationale for the sequence conservation of the loop nucleotides. The nucleotide identity of the highly conserved U307 and G309 has been shown to be important for activity, while that of the non-conserved G308 is not (24,25). The conserved P6.1 loop nucleotides have been proposed to be involved in an interaction with a template-adjacent region of the pseudoknot/core domain (60), and the Ψs may facilitate the positioning of the loop nucleotides for this interaction, potentially contributing to processivity. Alternatively, the Ψs may be important for overall P6.1 stem stability, but the additional stabilization may make the loop structure less optimal for P6.1 interaction with the pseudoknot/core domain or with TERT. The P6.1 stem is critical for catalytic activity and for TERT binding (24,25). Importantly, compensatory mutations that restore base pairing rescue TERT binding and catalytic activity, indicating that the formation of a stable stem structure is more important than stem sequence. Telomerase function *in vivo* requires a delicate balance of telomere lengthening in response to telomere degradation, and hTER Ψs could contribute to fine-tuning telomerase catalytic properties.

In vivo, Ψ modification is catalyzed by a family of proteins. Although some functional RNAs are modified site-specifically by a stand-alone Ψ synthase, the site-specificity of Ψ modification of most nuclear non-coding RNAs is established through base pairing to the RNA subunit of an H/ACA RNP enzyme. Notably, the region surrounding the conserved P6.1 loop nucleotide

(hTER U307) is absolutely conserved among vertebrate TERs. Compensatory substitutions of the absolutely conserved P6.1 stem nucleotides have no detectable effect on human or mouse telomerase catalytic activity assayed following reconstitution of overexpressed TERT and hTER *in vivo* or TERT and hTER fragments *in vitro* (24,25). Thus, the conservation of P6.1 primary sequence motif is not accounted for by biochemical requirements for telomerase function. The only non-conserved P6.1 residue (G308) is immediately 3' of the Ψ modification(s) in the P6.1 loop. For other non-coding RNAs that are pseudouridylated by H/ACA RNPs, the nucleotide 3' to the target U is the only one of the local 10 nt or more that is not involved in a contact with the guide RNA in the H/ACA RNP. In addition, the less conserved positions of the P6.1 motif (306, 310) are evolutionarily substituted in a manner that would retain base pairing of a modification guide RNA. We hypothesize that the sequence conservation in the P6.1 stem may be due to a combined selection for P6.1 loop Ψ modification and for base pairing of the P6.1 stem for telomerase function.

ACCESSION NUMBER

Coordinates and restraints for the 20 lowest energy structures of Ψ 4-P6.1 have been deposited in the Protein Data Bank under accession number 2kye.

SUPPLEMENTARY DATA

Supplementary Data are available at NAR Online.

ACKNOWLEDGEMENTS

The authors thank Prof. Julian J.-L. Chen and Mingyi Xie for training N.-K. Kim to do the direct telomerase assays, Dr Qi Zhang for providing the core domain of hTER, and Dr Robert Peterson for help with NMR spectroscopy.

FUNDING

National Institutes of Health (grants GM48123 and G37254 to J.F.); National Science Foundation (grant MCB 051770 to J.F.). Funding for open access charge: National Institutes of Health (grant GM48123 to J.F.).

Conflict of interest statement. None declared.

REFERENCES

- Cohn,W.E. (1960) Pseudouridine, a carbon-carbon linked ribonucleoside in ribonucleic acids: isolation, structure, and chemical characteristics. *J. Biol. Chem.*, **235**, 1488–1498.
- Hamma,T. and Ferre-D'Amare,A.R. (2006) Pseudouridine synthases. *Chem. Biol.*, **13**, 1125–1135.
- Charette,M. and Gray,M.W. (2000) Pseudouridine in RNA: what, where, how, and why. *IUBMB Life*, **49**, 341–351.
- Cabello-Villegas,J. and Nikonowicz,E.P. (2005) Solution structure of psi32-modified anticodon stem-loop of Escherichia coli tRNA^{Phe}. *Nucleic Acids Res.*, **33**, 6961–6971.
- Durant,D.R. (1995) Stabilization of RNA stacking by pseudouridine. *Nucleic Acids Res.*, **23**, 5020–5026.
- Durant,P.C. and Davis,D.R. (1999) Stabilization of the anticodon stem-loop of tRNA^{Lys,3} by an A+C base-pair and by pseudouridine. *J. Mol. Biol.*, **285**, 115–131.
- Bilbille,Y., Vendeix,F.A., Guenther,R., Malkiewicz,A., Ariza,X., Vilarrasa,J. and Agris,P.F. (2009) The structure of the human tRNA^{Lys3} anticodon bound to the HIV genome is stabilized by modified nucleosides and adjacent mismatch base pairs. *Nucleic Acids Res.*, **37**, 3342–3353.
- Newby,M.I. and Greenbaum,N.L. (2002) Investigation of Overhauser effects between pseudouridine and water protons in RNA helices. *Proc. Natl Acad. Sci. USA*, **99**, 12697–12702.
- Yang,C., McPheeters,D.S. and Yu,Y.T. (2005) Psi35 in the branch site recognition region of U2 small nuclear RNA is important for pre-mRNA splicing in Saccharomyces cerevisiae. *J. Biol. Chem.*, **280**, 6655–6662.
- Zhao,X. and Yu,Y.T. (2004) Pseudouridines in and near the branch site recognition region of U2 snRNA are required for snRNP biogenesis and pre-mRNA splicing in Xenopus oocytes. *RNA*, **10**, 681–690.
- Artandi,S.E. (2006) Telomeres, telomerase, and human disease. *N. Engl. J. Med.*, **355**, 1195–1197.
- Autexier,C. and Lue,N.F. (2006) The structure and function of telomerase reverse transcriptase. *Annu. Rev. Biochem.*, **75**, 493–517.
- Collins,K. (2008) Physiological assembly and activity of human telomerase complexes. *Mech. Ageing. Dev.*, **129**, 91–98.
- Collins,K. (2006) The biogenesis and regulation of telomerase holoenzymes. *Nat. Rev. Mol. Cell. Biol.*, **7**, 484–494.
- Theimer,C.A. and Feigon,J. (2006) Structure and function of telomerase RNA. *Curr. Opin. Struct. Biol.*, **16**, 307–318.
- Venteicher,A.S., Abreu,E.B., Meng,Z., McCann,K.E., Terns,R.M., Veenstra,T.D., Terns,M.P. and Artandi,S.E. (2009) A human telomerase holoenzyme protein required for Cajal body localization and telomere synthesis. *Science*, **323**, 644–648.
- Chen,J.L., Blasco,M.A. and Greider,C.W. (2000) Secondary structure of vertebrate telomerase RNA. *Cell*, **100**, 503–514.
- Chen,J.L. and Greider,C.W. (2004) An emerging consensus for telomerase RNA structure. *Proc. Natl Acad. Sci. USA*, **101**, 14683–14684.
- Dandjinou,A.T., Levesque,N., Larose,S., Lucier,J.F., Abou Elela,S. and Wellinger,R.J. (2004) A phylogenetically based secondary structure for the yeast telomerase RNA. *Curr. Biol.*, **14**, 1148–1158.
- Theimer,C.A., Blois,C.A. and Feigon,J. (2005) Structure of the human telomerase RNA pseudoknot reveals conserved tertiary interactions essential for function. *Mol. Cell*, **17**, 671–682.
- Qiao,F. and Cech,T.R. (2008) Triple-helix structure in telomerase RNA contributes to catalysis. *Nat. Struct. Mol. Biol.*, **15**, 634–640.
- Mitchell,J.R. and Collins,K. (2000) Human telomerase activation requires two independent interactions between telomerase RNA and telomerase reverse transcriptase. *Mol. Cell*, **6**, 361–371.
- Ly,H., Blackburn,E.H. and Parslow,T.G. (2003) Comprehensive structure-function analysis of the core domain of human telomerase RNA. *Mol. Cell. Biol.*, **23**, 6849–6856.
- Chen,J.L., Opperman,K.K. and Greider,C.W. (2002) A critical stem-loop structure in the CR4-CR5 domain of mammalian telomerase RNA. *Nucleic Acids Res.*, **30**, 592–597.
- Robart,A.R. and Collins,K. (2010) Investigation of human telomerase holoenzyme assembly, activity, and processivity using disease-linked subunit variants. *J. Biol. Chem.*, **285**, 4375–4386.
- Fu,D. and Collins,K. (2003) Distinct biogenesis pathways for human telomerase RNA and H/ACA small nucleolar RNAs. *Mol. Cell*, **11**, 1361–1372.
- Collins,K. and Mitchell,J.R. (2002) Telomerase in the human organism. *Oncogene*, **21**, 564–579.
- Theimer,C.A., Jady,B.E., Chim,N., Richard,P., Breece,K.E., Kiss,T. and Feigon,J. (2007) Structural and functional characterization of human telomerase RNA processing and cajal body localization signals. *Mol. Cell*, **27**, 869–881.
- Cristofari,G., Adolf,E., Reichenbach,P., Sikora,K., Terns,R.M., Terns,M.P. and Lingner,J. (2007) Human telomerase RNA accumulation in Cajal bodies facilitates telomerase recruitment to telomeres and telomere elongation. *Mol. Cell*, **27**, 882–889.

30. Tesmer, V.M., Ford, L.P., Holt, S.E., Frank, B.C., Yi, X., Aisner, D.L., Ouellette, M., Shay, J.W. and Wright, W.E. (1999) Two inactive fragments of the integral RNA cooperate to assemble active telomerase with the human protein catalytic subunit (hTERT) in vitro. *Mol. Cell. Biol.*, **19**, 6207–6216.
31. Moriarty, T.J., Marie-Egyptienne, D.T. and Autexier, C. (2004) Functional organization of repeat addition processivity and DNA synthesis determinants in the human telomerase multimer. *Mol. Cell. Biol.*, **24**, 3720–3733.
32. Leeper, T., Leulliot, N. and Varani, G. (2003) The solution structure of an essential stem-loop of human telomerase RNA. *Nucleic Acids Res.*, **31**, 2614–2621.
33. Mitchell, J.R., Wood, E. and Collins, K. (1999) A telomerase component is defective in the human disease dyskeratosis congenita. *Nature*, **402**, 551–555.
34. Bakin, A. and Ofengand, J. (1993) Four newly located pseudouridylate residues in Escherichia coli 23S ribosomal RNA are all at the peptidyltransferase center: analysis by the application of a new sequencing technique. *Biochemistry*, **32**, 9754–9762.
35. Gullerez, J., Lopez, P.J., Proux, F., Launay, H. and Dreyfus, M. (2005) A mutation in T7 RNA polymerase that facilitates promoter clearance. *Proc. Natl Acad. Sci. USA*, **102**, 5958–5963.
36. Cromsigt, J., van Buuren, B., Schleucher, J. and Wijmenga, S. (2001) Resonance assignment and structure determination for RNA. *Methods Enzymol.*, **338**, 371–399.
37. Dieckmann, T. and Feigon, J. (1997) Assignment methodology for larger RNA oligonucleotides: application to an ATP-binding RNA aptamer. *J. Biomol. NMR*, **9**, 259–272.
38. Peterson, R.D., Theimer, C.A., Wu, H. and Feigon, J. (2004) New applications of 2D filtered/edited NOESY for assignment and structure elucidation of RNA and RNA-protein complexes. *J. Biomol. NMR*, **28**, 59–67.
39. Cavanagh, J. and Rance, M. (1990) Sensitivity improvement in isotropic mixing (TOCSY) experiments. *J. Magn. Reson.*, **88**, 72–85.
40. Piotto, M., Saudek, V. and Sklenar, V. (1992) Gradient-tailored excitation for single-quantum NMR spectroscopy of aqueous solutions. *J. Biomol. NMR*, **2**, 661–665.
41. Hennig, M., Fohrer, J. and Carlomagno, T. (2005) Assignment and NOE analysis of 2'-hydroxyl protons in RNA: implications for stabilization of RNA A-form duplexes. *J. Am. Chem. Soc.*, **127**, 2028–2029.
42. Kay, L.E., Keifer, P. and Saarinen, T. (1992) Pure absorption gradient enhanced heteronuclear single quantum correlation spectroscopy with improved sensitivity. *J. Am. Chem. Soc.*, **114**, 10663–10665.
43. Legault, P., Jucker, F.M. and Pardi, A. (1995) Improved measurement of ¹³C, ³¹P J coupling constants in isotopically labeled RNA. *FEBS Lett.*, **362**, 156–160.
44. Kim, N.K., Zhang, Q., Zhou, J., Theimer, C.A., Peterson, R.D. and Feigon, J. (2008) Solution structure and dynamics of the wild-type pseudoknot of human telomerase RNA. *J. Mol. Biol.*, **384**, 1249–1261.
45. Wijmenga, S.S., Heus, H.A., Werten, B., van der Marel, G.A., van Boom, J.H. and Hilbers, C.W. (1994) Assignment strategies and analysis of cross-peak patterns and intensities in the three-dimensional homonuclear TOCSY-NOESY of RNA. *J. Magn. Reson. B*, **103**, 134–141.
46. Koradi, R., Billeter, M. and Wuthrich, K. (1996) MOLMOL: a program for display and analysis of macromolecular structures. *J. Mol. Graph.*, **14**, 29–32, 51–55.
47. Theimer, C.A., Wang, Y., Hoffman, D.W., Krisch, H.M. and Giedroc, D.P. (1998) Non-nearest neighbor effects on the thermodynamics of unfolding of a model mRNA pseudoknot. *J. Mol. Biol.*, **279**, 545–564.
48. Xie, M., Mosig, A., Qi, X., Li, Y., Stadler, P.F. and Chen, J.J. (2008) Structure and function of the smallest vertebrate telomerase RNA from teleost fish. *J. Biol. Chem.*, **283**, 2049–2059.
49. Chen, J.L. and Greider, C.W. (2005) Functional analysis of the pseudoknot structure in human telomerase RNA. *Proc. Natl Acad. Sci. USA*, **102**, 8080–8085.
50. Durant, P.C., Bajji, A.C., Sundaram, M., Kumar, R.K. and Davis, D.R. (2005) Structural effects of hypermodified nucleosides in the Escherichia coli and human tRNALys anticodon loop: the effect of nucleosides s2U, mcm5U, mcm5s2U, mnm5s2U, t6A, and ms2t6A. *Biochemistry*, **44**, 8078–8089.
51. Lin, Y. and Kielkopf, C.L. (2008) X-ray structures of U2 snRNA-branchpoint duplexes containing conserved pseudouridines. *Biochemistry*, **47**, 5503–5514.
52. Newby, M.I. and Greenbaum, N.L. (2001) A conserved pseudouridine modification in eukaryotic U2 snRNA induces a change in branch-site architecture. *RNA*, **7**, 833–845.
53. Yarian, C.S., Basti, M.M., Cain, R.J., Ansari, G., Guenther, R.H., Sochacka, E., Czerwinska, G., Malkiewicz, A. and Agris, P.F. (1999) Structural and functional roles of the N1- and N3-protons of psi at tRNA's position 39. *Nucleic Acids Res.*, **27**, 3543–3549.
54. Meroueh, M., Grohar, P.J., Qiu, J., SantaLucia, J. Jr, Scaringe, S.A. and Chow, C.S. (2000) Unique structural and stabilizing roles for the individual pseudouridine residues in the 1920 region of Escherichia coli 23S rRNA. *Nucleic Acids Res.*, **28**, 2075–2083.
55. Podlevsky, J.D., Bley, C.J., Omana, R.V., Qi, X.D. and Chen, J.J.L. (2008) The telomerase database. *Nucleic Acids Res.*, **36**, D339–D343.
56. Ennifar, E., Nikulin, A., Tishchenko, S., Serganov, A., Nevskaya, N., Garber, M., Ehresmann, B., Ehresmann, C., Nikonov, S. and Dumas, P. (2000) The crystal structure of UUCG tetraloop. *J. Mol. Biol.*, **304**, 35–42.
57. Allain, F.H. and Varani, G. (1995) Structure of the P1 helix from group I self-splicing introns. *J. Mol. Biol.*, **250**, 333–353.
58. Chen, J.L. and Greider, C.W. (2003) Template boundary definition in mammalian telomerase. *Genes Dev.*, **17**, 2747–2752.
59. Brown, Y., Abraham, M., Pearl, S., Kabaha, M.M., Elboher, E. and Tzfati, Y. (2007) A critical three-way junction is conserved in budding yeast and vertebrate telomerase RNAs. *Nucleic Acids Res.*, **35**, 6280–6289.
60. Ueda, C.T. and Roberts, R.W. (2004) Analysis of a long-range interaction between conserved domains of human telomerase RNA. *RNA*, **10**, 139–147.
61. Wang, F., Podell, E.R., Zaug, A.J., Yang, Y.T., Baciou, P., Cech, T.R. and Lei, M. (2007) The POT1-TPP1 telomere complex is a telomerase processivity factor. *Nature*, **445**, 506–510.